Modeling of the Postyield Response of Glassy Polymers: Influence of Thermomechanical History

E. T. J. Klompen, T. A. P. Engels, L. E. Govaert,* and H. E. H. Meijer

Section Materials Technology (MaTe), Dutch Polymer Institute (DPI), Eindhoven University of Technology, P.O. Box 513, NL-5600 MB, Eindhoven, The Netherlands

Received March 8, 2005; Revised Manuscript Received May 26, 2005

ABSTRACT: The continuous development of constitutive equations for the finite strain deformation of glassy polymers has resulted in a number of sophisticated models that can accurately capture the materials' intrinsic behavior. Numerical simulations using these models revealed that the thermal history plays a crucial role in the macroscopic deformation. Generally, macroscopic behavior is assumed not to change during a test, however, for certain test conditions this does not hold and a relevant change in mechanical properties, known as physical aging, can be observed. To investigate the consequences of this change in material structure, the existing models are modified and enhanced by incorporating an aging term, and its parameters are determined. The result is a validated constitutive relation that is able to describe the deformation behavior of, in our case, polycarbonate over a large range of molecular weights and thermal histories, with one parameter set only.

1. Introduction

In the past few decades considerable attention has been awarded to the development of constitutive relations for the large strain deformation of solid polymeric materials.[1−5] These efforts were motivated by the desire to predict mechanical properties and performance and to develop (numerical) tools for better understanding and, finally, improving properties of homogeneous, as well as heterogeneous, polymer systems.[6]

A landmark in this area of research is the original paper of Haward and Thackray from 1968,[1] where they proposed to govern the large strain deformation of polymers below their glass transition temperature by two separate processes. The first process reflects the rate-dependent plastic flow related to temperature and stress-activated motion of chain segments, which is represented by an Eyring viscosity.[7] The second process is related to the molecular alignment resulting from the plastic flow process and is modeled using a finite extendable spring (a so-called Langevin spring) following the conventional theory of rubber elasticity.[8]

The Haward and Thackray model was extended to a fully 3-D description by Boyce, Parks and Argon,[2] in what is now known as the *BPA model*. In this model, the plastic flow contribution is described by a 3-D representation of the Argon flow theory,[9] including pressure dependence and a phenomenological description of intrinsic strain softening. The entropic hardening is modeled by using the three-chain model of Wang and Guth,[10] later improved by the more realistic eight chain model, Arruda and Boyce.[11] A modification of the BPA-model was proposed by Wu and van der Giessen,[3] replacing the 3-chain model with a full network model (the *full-chain model*).

An alternative approach was presented by Tervoort et al.,[12] who formulated a 3-D model for nonlinear viscoelastic behavior based on a compressible version of Leonov's fluid model[13] as originally proposed by Baaijens.[14] The resulting elastoviscoplastic model, with two basic elements—a linear elastic spring and a 3-D Eyring dashpot—was further refined by Govaert et al.[5] by adding pressure dependence and (phenomenological) softening based on the concept of Hasan et al.,[15] and a neo-Hookean rubber spring representing strain hardening, as suggested by Tervoort and Govaert.[16]

These models were among others used in the investigation of strain localization phenomena in polymers such as shear banding, necking, and crazing.[5,17,18] From these numerical investigations it became evident that the occurrence of these phenomena is completely captured by the polymers' intrinsic behavior. Initiation of localization is caused by the intrinsic strain softening, whereas the way this localized zone evolves depends on the stabilizing effect of strain hardening.[17−19] Ultimately the balance between strain softening and hardening determines whether a polymer deforms macroscopically ductile (stable), or brittle (unstable).[20]

These numerical findings were supported by experimental observations, which showed that a change in softening can have dramatic effects on the macroscopic behavior. Such a change can be realized by application of thermal or mechanical treatments. The resulting thermomechanical history, however, only influences the yield stress, since the final rejuvenated state is known to be independent of any prior history.[15,20,21] Quenching a sample for instance, results in a lower yield stress leading to less softening in a compression test and less localized deformation in a tensile test. A prime example of this is reported by Cross and Haward[22] who observed uniform deformation for quenched poly(vinyl chloride) samples, whereas slowly cooled samples developed a neck. Various authors showed that by mechanical preconditioning, or predeformation, the amount of strain softening can be reduced or even eliminated.[5,23−25] This pretreatment results in uniform deformation of polycarbonate (no neck),[5] and it even induces complete ductile deformation in polystyrene (no crazing).[25] Increasing the amount of softening by increasing the yield stress, on the other hand, e.g., by annealing, leads to severe localization of strain and can even induce brittle fracture in (relatively low molecular weight) polycarbonate.[20,26−28]

* Corresponding author. E-mail: l.e.govaert@tue.nl.

10.1021/ma050498v CCC: $30.25
Published on Web 07/08/2005

Table 1. Number-Averaged and Weight-Averaged Molecular Weights of the Polycarbonate Grades Used in This Study Measured with Respect to a PC-Standard

grade	M_n [kg/mol]	M_w [kg/mol]
Lexan OQ1050	8.1	16.8
Makrolon CD2000	8.2	18.7
Lexan 141R	9.2	25.8
Lexan 121R	9.8	23.4
Lexan 161R	11.6	27.9
Lexan 101R	12.7	28.9
extruded rod	14.0	35.9

In modeling practice and in experiments, it is usually assumed that the initial age exceeds the experimental time which implies that material properties do not change and are time invariant during the test. In the case of long-term loading conditions, or conditions where accelerated aging can be expected, e.g. at high temperatures, this assumption might no longer hold and, consequently, the parameters will change during the experiment: *progressive aging*.[29] At room-temperature such a spontaneous increase of the yield stress is indeed observed experimentally, in particular with samples where the softening is reduced through a thermal, or mechanical, treatment. For quenched PVC samples at room temperature the yield stress was seen to increase with time by Cross and Haward[22] and by Struik.[29] Van Melick et al.[30] reported an increasing yield stress at room temperature after mechanical predeformation of polystyrene, leading to reembrittlement within a time scale of hours. In addition it was shown that the kinetics involved depend on the material and are accelerated at elevated temperatures. For both as-received samples,[26,31−33] as well as rejuvenated samples,[34,35] the yield stress is seen to increase with time and annealing temperature.

To account for such changes in yield stress, and thus changes in softening, the model should include a time-dependent yield stress. To describe such behavior, an extension of the current elastoviscoplastic models is proposed and the relevant characteristics and parameters are experimentally determined using polycarbonate as model material. Application of the model to long-term loading will be dealt with in a separate publication.

2. Experimental Section

2.1. Materials. Different grades of polycarbonate were used, including Bayer Makrolon CD2000 and General Electric Lexan OQ1050, 101R, 121R, 141R, and 161R. Apart from these materials, which were supplied as granules, also an extrusion grade of Lexan (type unknown), supplied as 6 mm diameter extruded rod, was studied. Molecular weight distributions were determined using gel permeation chromatography (GPC), and the resulting number-averaged and weight-averaged molecular weights are tabulated in Table 1.

For uniaxial compression tests, cylindrical samples (o.d. 6 mm × 6 mm) were machined from either the extruded rod or from plates (200 × 200 × 10 mm^3) that were compression molded from granular material at a temperature of 250 °C. First the dried granulate was heated for 15 min and next compressed up to 300 kN in five subsequent intervals of 5 min. After each step the force was released to allow for degassing. Finally, the mold was placed in a cold press and cooled to room temperature (20 °C) under a moderate force (100 kN). Tensile samples were prepared either through injection molding, or milled from compression molded plates (160 × 160 × 3 mm^3) (molded also according to the procedure outlined above). Geometry of all tensile specimens was according to ISO 527.

2.2. Thermomechanical Treatments. Annealing of samples was performed for different periods of time in an air circulated oven at various temperatures (80−130 °C). Initial equilibration of the sample temperature was measured to be approximately 15 min. After a predefined time, the samples were removed from the oven and allowed to cool to room temperature in air before being tested.

Mechanical preconditioning was performed both in the preyield and postyield range. The latter involved mechanical rejuvenation of specimens by either torsion or rolling. With torsion, cylindrical samples were twisted to-and-fro over a twist angle of 1150°, whereas with rolling, samples were run through a two-roll mill (o.d. 45 mm), yielding a thickness reduction of about 10%. In the preyield range samples were preconditioned under constant force on either a Zwick Rel servo-hydraulic tensile tester equipped with a temperature chamber or a long-term dead-weight setup at room temperature for different amounts of time. Samples were tested after a short equilibration time.

A number of samples was subjected to a combined thermal and mechanical history, consisting of a constant applied load at different temperatures for various amounts of time. After this time the samples were unloaded and allowed to cool to room-temperature in air prior to testing.

2.3. Mechanical Testing. Uniaxial compression tests were performed on a servo-hydraulic MTS Elastomer Testing System 810. The specimens were cylindrical shaped and compressed under true strain control, at constant true strain rates of 10^{-4}−10^{-2} s^{-1} between two parallel, flat steel plates. Friction between samples and plates was reduced by an empirically optimized method. Onto the sample ends a thin film of PTFE tape (3M 5480, PTFE skived film tape) was applied and the contact area between steel and tape was lubricated using a 1:1 mixture of liquid soap and water. During the test no bulging of the sample was observed, indicating that the friction was sufficiently reduced.

Tensile tests were performed on a Zwick Z010 tensile tester, at constant linear strain rate of 10^{-4}−10^{-2} s^{-1}, at distinct aging times after predeformation. Besides the stress−strain curve, the yield stress was recorded. True stresses were calculated assuming a constant sample volume.

3. Numerical Modeling

3.1. Constitutive Model. In the constitutive model used, a distinction is made concerning the contribution of secondary interactions between polymer chains, which determine the (visco-) elastic properties at small deformations and plastic flow, and the entangled polymer network, which governs strain hardening.[5]

Accordingly, the total Cauchy stress $\boldsymbol{\sigma}$ is decomposed into a driving stress $\boldsymbol{\sigma}_s$, and a hardening stress $\boldsymbol{\sigma}_r$:

$$\boldsymbol{\sigma} = \boldsymbol{\sigma}_s + \boldsymbol{\sigma}_r \tag{1}$$

Hardening is modeled with a neo-Hookean relation:[16]

$$\boldsymbol{\sigma}_r = G_r \tilde{\boldsymbol{B}}^d \tag{2}$$

Here G_r is the strain hardening modulus and $\tilde{\boldsymbol{B}}^d$ is the deviatoric part of the isochoric left Cauchy−Green deformation tensor.

The driving stress is decomposed into a deviatoric stress $\boldsymbol{\sigma}_s^d$, and a hydrostatic stress $\boldsymbol{\sigma}_s^h$:

$$\boldsymbol{\sigma}_s^d = G\tilde{\boldsymbol{B}}_e^d \quad \text{and} \quad \boldsymbol{\sigma}_s^h = \kappa(J-1)\boldsymbol{I} \tag{3}$$

where G is the shear modulus, $\tilde{\boldsymbol{B}}_e^d$ the deviatoric part of the isochoric elastic left Cauchy−Green strain tensor, κ the bulk modulus, J the volume change factor, and $\boldsymbol{I}$

the unity tensor. The evolution of J and $\tilde{\boldsymbol{B}}_e^d$ is given by the following equations:

$$\dot{J} = J\,\mathrm{tr}(\boldsymbol{D}) \tag{4}$$

$$\mathring{\tilde{\boldsymbol{B}}}_e = (\boldsymbol{D}^d - \boldsymbol{D}_p)\cdot\tilde{\boldsymbol{B}}_e + \tilde{\boldsymbol{B}}_e\cdot(\boldsymbol{D}^d - \boldsymbol{D}_p) \tag{5}$$

Here $\mathring{\tilde{\boldsymbol{B}}}_e$ is the Jaumann rate of $\tilde{\boldsymbol{B}}_e$, $\boldsymbol{D}^d$ the deviatoric part of the rate of deformation tensor, and $\boldsymbol{D}_p$ the plastic part of the rate of deformation tensor.

A non-Newtonian flow rule with a stress-dependent Eyring viscosity is used to relate the plastic deformation rate tensor, $\boldsymbol{D}_p$, to the deviatoric driving stress, $\boldsymbol{\sigma}_s^d$:[12]

$$\boldsymbol{D}_p = \frac{\boldsymbol{\sigma}_s^d}{2\eta(T, p, \bar{\tau}, D)} \tag{6}$$

The viscosity, η, strongly depends on the equivalent stress, $\bar{\tau}$, and was originally described by an Eyring relationship.[12] Govaert et al.[5] extended the model by incorporating pressure dependence (μ) and intrinsic strain softening (D) in the viscosity function:

$$\eta(T, p, \bar{\tau}, D) = A_0(T)\tau_0 \exp\left(\frac{\mu p}{\tau_0}\right)\frac{\bar{\tau}/\tau_0}{\sinh(\bar{\tau}/\tau_0)}\exp(-D) \tag{7}$$

Here the temperature-dependent preexponential factor $A_0(T)$ equals

$$A_0(T) = A_0 \exp\left(\frac{\Delta U}{RT}\right) \tag{8}$$

with A_0 a constant, ΔU the activation energy, R the gas constant, and T the absolute temperature. The characteristic stress τ_0, pressure p, and equivalent stress $\bar{\tau}$ are defined as

$$\tau_0 = \frac{kT}{V^*} \tag{9}$$

$$p = -\frac{1}{3}\mathrm{tr}(\boldsymbol{\sigma}) \tag{10}$$

$$\bar{\tau} = \sqrt{\frac{1}{2}\mathrm{tr}(\boldsymbol{\sigma}_s^d\boldsymbol{\sigma}_s^d)} \tag{11}$$

with V^* the activation volume, and k Boltzmann's constant.

The intrinsic strain softening is represented by the (structural) parameter D, which evolves from an initial value D_0 to an equilibrium value $D_\infty > D_0$ with increasing equivalent plastic strain $\bar{\gamma}_p$, thereby strongly reducing the material's viscosity η. This evolution is represented by

$$\dot{D} = h\left(1 - \frac{D}{D_\infty}\right)\dot{\bar{\gamma}}_p \tag{12}$$

where the material constant h represents the relative softening rate, and the equivalent plastic strain-rate $\dot{\bar{\gamma}}_p$ is provided by the following equation:

$$\dot{\bar{\gamma}}_p = \sqrt{2\,\mathrm{tr}(\boldsymbol{D}_p\cdot\boldsymbol{D}_p)} \tag{13}$$

In the original form of eq 12, as proposed by Hasan et al.,[15] the parameter D represents the *density of shear transformation sites*, which is derived from positron annihilation lifetime spectroscopy (PALS) measurements. Since the initial value D_0 depends on thermal history, a new value has to be determined for each sample with a different thermal history using either PALS measurements or a numerical fit.

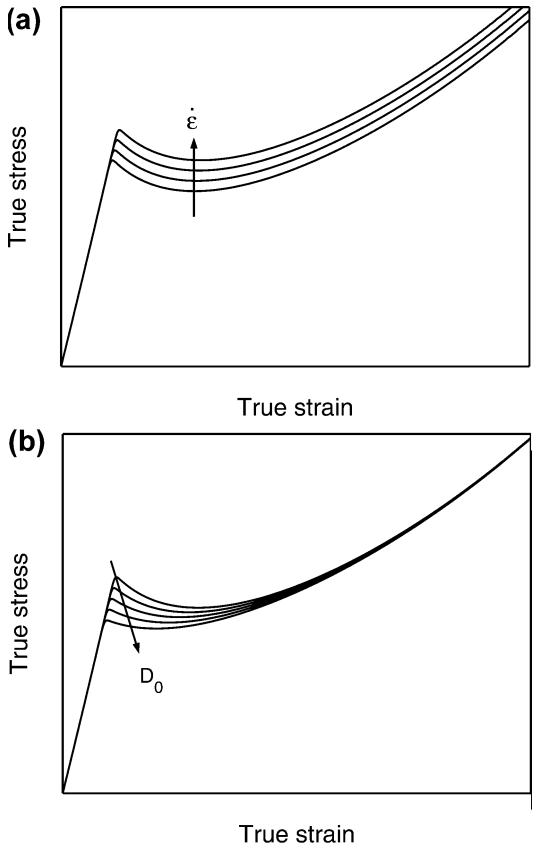

Figure 1. Schematic representation of the response of the elastoviscoplastic model to uniaxial extension at different strain rates (a), and for different initial states D_0 (b).

To illustrate some of the characteristic features of the model, Figure 1a shows its response to different strain rates. The initial linear elastic deformation is followed by a strain rate dependent yield point, while the postyield behavior (both softening and hardening) is strain rate independent. This behavior is found, e.g., in experimental observations on polycarbonate.[36] Figure 1b shows the effect of different initial states. Yield stress, and the amount of softening can be seen to decrease with an increasing value of D_0. The response at large deformations is independent of the initial state, which corresponds to the experimentally observed deformation induced erasure of thermomechanical history (mechanical rejuvenation).[15,20,21]

3.2. Incorporation of Aging Kinetics. From Figure 1b it is clear that the initial condition D_0 can be used to describe the yield stress induced by different thermomechanical histories. Using a first-order evolution, an increasing yield stress with time can, however, not be obtained, e.g., by letting D_0 evolve with time, since the initial condition only has an effect on $t = 0$. This was also recognized by Hasan et al.,[15] who therefore schematically proposed an extension by adding an additional term representing the aging behavior. Dependence of temperature, pressure, and structural state was suggested, but no explicit expression was given. Under the assumption that the initial age exceeds the experimental time under consideration the term was neglected anyway. As pointed out in the Introduction there are however circumstances, e.g., a small initial age or

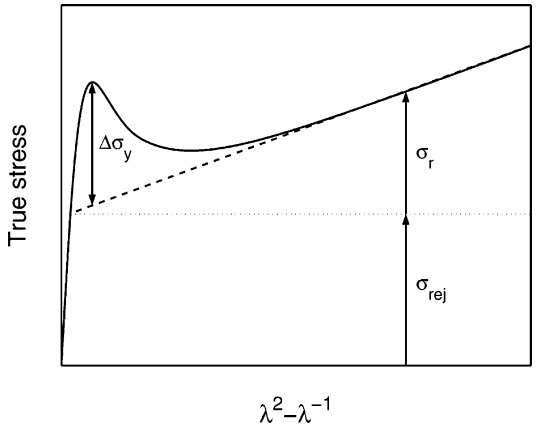

Figure 2. Schematic representation of the decomposition of the true stress in three separate contributions.

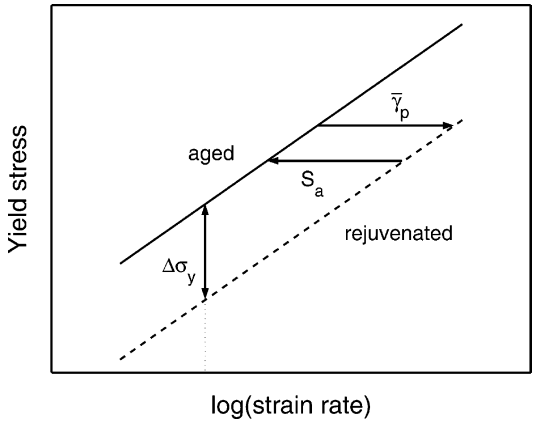

Figure 3. Schematic representation of the evolution of yield stress with time, and plastic strain for different strain rates.

elevated temperatures, where this assumption does not hold.

In a first attempt to enable a combined description of relevant aging and softening kinetics, a simplified approach is proposed here. Essence is the decomposition of the intrinsic flow stress σ in three components, see Figure 2, similar to an approach proposed by G'Sell:[23]

$$\sigma(\dot{\epsilon}, S, \epsilon) = \sigma_{rej}(\dot{\epsilon}) + \Delta\sigma_y(S) + \sigma_r(\epsilon) \qquad (14)$$

Together with the history independent flow stress σ_{rej} of the fully rejuvenated state, the strain hardening stress σ_r represents the steady state, or homogeneous deformation behavior of the material.[23] The remaining transient component, the yield drop $\Delta\sigma_y$, depends on the thermomechanical history of the material, represented by the state parameter S. With regard to the yield drop, it is assumed that it is independent of both strain rate and test temperature, which for polycarbonate at moderate temperatures is a fair assumption.[36]

In terms of the previously described elastoviscoplastic model, this decomposition can be easily realized by modifying the viscosity definition (eq 7) to that of the rejuvenated state:

$$\eta(T, p, \bar{\tau}) = \eta_{0,r}(T) \exp\left(\frac{\mu p}{\tau_0}\right) \frac{\bar{\tau}/\tau_0}{\sinh(\bar{\tau}/\tau_0)} \qquad (15)$$

where $\eta_{0,r}(T) = A_{rej}(T)\cdot\tau_0$, with $A_{rej}(T)$ the $A_0(T)$ value for rejuvenated material, and τ_0, p, and $\bar{\tau}$ are defined by eqs 9−11. As can be seen, the resulting flow stress depends on temperature, pressure, and rate, but not on history. When this definition is applied, homogeneous deformation is predicted. The desired history dependence is added by introducing the state parameter S into eq 15:

$$\eta(T, p, \bar{\tau}, S) = \eta_{0,r}(T) \exp\left(\frac{\mu p}{\tau_0}\right) \frac{\bar{\tau}/\tau_0}{\sinh(\bar{\tau}/\tau_0)} \exp(S) \qquad (16)$$

To a first approximation, the evolution of parameter S is assumed to be

$$S(t, T, \bar{\gamma}_p) = S_a(t, T)\, R_\gamma(\bar{\gamma}_p) \qquad (17)$$

Here $S_a(t, T)$ represents the aging kinetics depending on time and temperature, whereas the softening kinetics $R_\gamma(\bar{\gamma}_p)$ are determined by the equivalent plastic strain. Furthermore, it is assumed that the initial value of parameter S is entirely determined by S_a, while the magnitude of $R_\gamma(\bar{\gamma}_p)$, normalized to 1, decreases monotonically to 0 with increasing (equivalent) plastic strain. Similar to Govaert et al.,[5] S is used as a fitting parameter rather than a true physical parameter.

In contrast to the work of Govaert et al.,[5] where D *reduces* an arbitrary history-dependent viscosity, in this approach S *increases* the fixed rejuvenated viscosity. This is demonstrated schematically in Figure 3, which shows the strain-rate dependent yield stress resulting from eqs 16 and 17. The yield stress can be seen to evolve from the rejuvenated reference level to its momentary value through the function S_a, whereas applying plastic deformation reduces the momentary yield stress to the rejuvenated reference level.

With regard to the definition of the state parameter S it should be noted that the effects of aging and rejuvenation are decoupled. This has the advantage that the relevant kinetics can be determined more easily. In reality, however, both kinetics depend on the momentary state of the material.

In the following section, the relevant characteristics, kinetics, and material parameters are experimentally determined and validated.

4. Results

Two main parts are distinguished: the first concerns the derivation and validation of the intrinsic behavior, more particularly the softening kinetics $R_\gamma(\bar{\gamma}_p)$, whereas the second concerns the aging kinetics $S_a(t, T)$ and its validation.

4.1. Characterization of Intrinsic Behavior. To determine the intrinsic deformation behavior, a loading geometry that inhibits the occurrence of strain localization during the experiment has to be utilized. The most convenient solution is using a uniaxial compression test. Figure 4 shows the intrinsic behavior of polycarbonate Lexan 121R determined in compression at a true strain rate of 10^{-3} s^{-1}. Following the yield point at a relatively small strain, the material shows true strain softening, and at large deformations, strain hardening sets in.

Assuming that the initial age of the sample is considerably larger than the experimental time scale, no aging occurs during this experiment, i.e., S_a in eq 17 is constant. From eq 14, it follows that the total stress is made up of three main contributions: the rejuvenated stress, the yield drop, and the hardening stress. As-

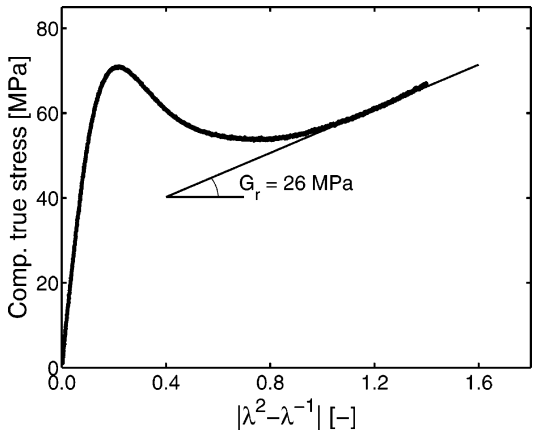

Figure 4. Intrinsic deformation behavior of PC Lexan 121R measured in compression at a true compressive strain-rate of 10^{-3} s^{-1}.

suming incompressible behavior during plastic deformation, the driving stress σ_s ($= \sigma_{rej} + \Delta\sigma_y$) is given by

$$\sigma_s = \sigma - \sigma_r = \sigma - G_r(\lambda^2 - \lambda^{-1}) \tag{18}$$

where σ is the experimentally determined true stress, σ_r the hardening stress, which is determined by the rubber modulus G_r, and draw ratio λ. The value of the strain hardening modulus is taken from Tervoort and Govaert et al.,[16] who obtained a strain hardening modulus for polycarbonate of 26 MPa from three different loading geometries. As seen in Figure 4, this value gives a good description of the experimentally determined large strain behavior.

The resulting driving stress σ_s, shown in Figure 5a, can be split into the contributions of the history independent rejuvenated stress σ_{rej} and the history dependent transient yield drop $\Delta\sigma_y$:

$$\sigma_s(\dot{\epsilon}, S) = \sigma_{rej}(\dot{\epsilon}) + \Delta\sigma_y(S) \tag{19}$$

Equation 19 shows that this leads to a separation of strain rate and history dependence.

In eq 17, S_a determines the magnitude of S and thus the height of the yield drop $|\Delta\sigma_y|$, since at the yield point R_γ is taken to be equal 1. Therefore, we can obtain the softening characteristic simply from

$$R_\gamma(\bar{\gamma}_p) = \frac{\sigma_s - \sigma_{rej}}{|\Delta\sigma_y|} \tag{20}$$

where the equivalent plastic strain for uniaxial compression follows from integration of eq 13: $\bar{\gamma}_p = \sqrt{3}|\dot{\epsilon}|(t - t_y)$, assuming that plastic deformation starts at the yield point. The resulting experimentally determined softening characteristic is shown in Figure 5b (symbols).

Having isolated the experimental softening characteristic, a suitable expression to describe the data can be selected. We propose a modified version of the Carreau−Yassuda function:[37]

$$R_\gamma(\bar{\gamma}_p) = \frac{(1 + (r_0 \exp(\bar{\gamma}_p))^{r_1})^{(r_2-1)/r_1}}{(1 + r_0{}^{r_1})^{(r_2-1)/r_1}} \tag{21}$$

Here $\bar{\gamma}_p$ is the equivalent plastic strain, and r_0, r_1, and r_2 are fit parameters. Figure 5b shows that this expression provides a good description over the whole range of strains, and it will therefore be adopted for further use.

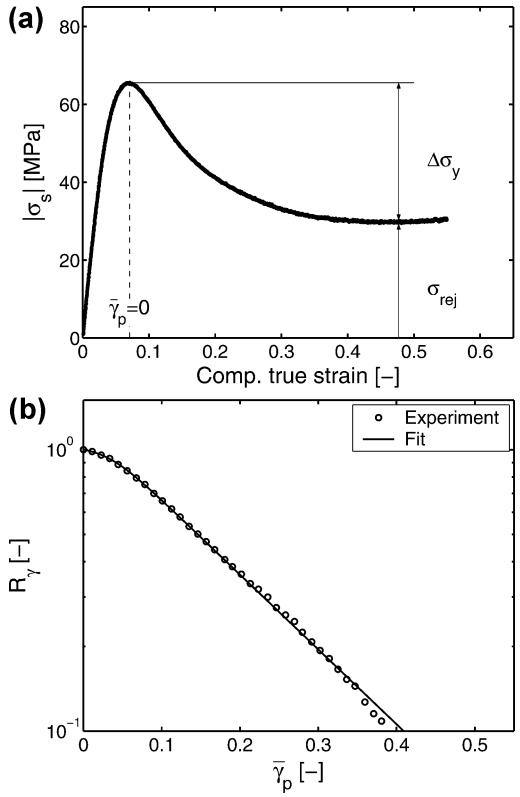

Figure 5. (a) Resulting driving stress component after removal of strain hardening. Also indicated are the steady-state rejuvenated, and transient part. (b) Softening characteristic R_γ vs equivalent plastic strain determined from a uniaxial compression experiment. Symbols (○) are experimental data, and the solid line is a fit using eq 21.

Besides the parameters for softening, the model requires the determination of several other parameters. Most of them can be determined from fitting the results of uniaxial compression tests at different strain rates. This is specifically the case for the parameters τ_0 and $\eta_{0,r}$, which determine the rate dependence of the plastic flow response of the rejuvenated material and for the strain hardening modulus G_r. Also the parameters governing the softening kinetics (r_0, r_1, r_2), and the initial value of S_a can be determined directly in such a fitting procedure. A proven strategy is to start by fitting the response of a rejuvenated material ($S_a = 0$) on the strain hardening regime of the experimental curves giving values for τ_0, $\eta_{0,r}$, and G_r. Next, the softening can be added.

Finally, the three last parameters have to be found: the elastic modulus E, the Poisson ratio ν, and the pressure dependence μ. In the present, single mode, approach, the elastic modulus is chosen slightly too low such that the yield strain of the model approximately equals the experimentally observed strain-at-yield. In the case of polycarbonate this yielded a value of 900 MPa. The Poisson ratio ν can be determined by monitoring the transverse strain in a uniaxial tension or compression test, for polycarbonate a value of 0.4 was found.[12] The most commonly encountered method to obtain the pressure dependence μ is by measuring the strain rate dependence of the yield stress in different loading geometries (e.g., uniaxial, or planar, tension and compression, shear, etc.).[28,38,39] The disadvantage of this

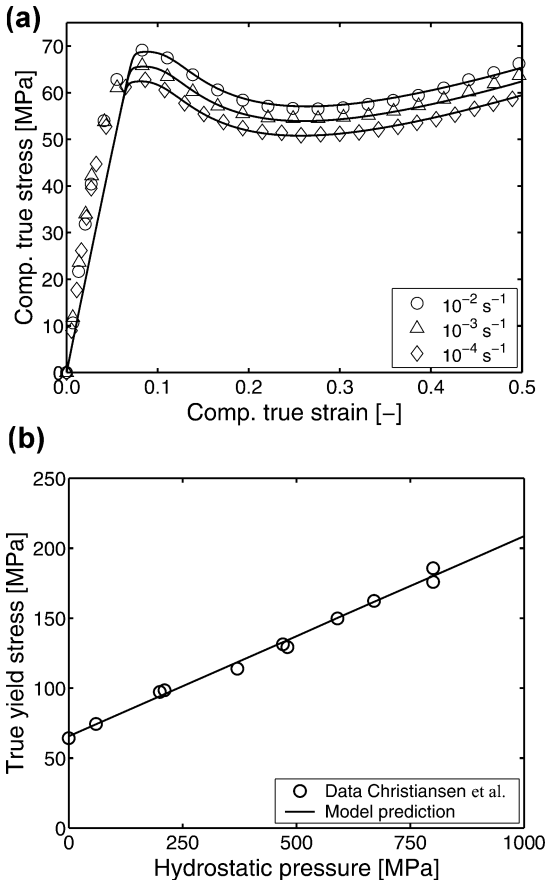

Figure 6. (a) True stress vs true strain in uniaxial compression, model prediction (solid lines) compared to experimental results (symbols), for different strain rates. (b) True yield stress vs applied hydrostatic pressure, model prediction (solid line) compared to experimental results (symbols) by Christiansen et al.[41] at a strain rate of 1.7×10^{-4} s^{-1}.

method is that each geometry requires its own, optimized, sample shape and dimensions. In particular the latter can have a strong influence on the thermal history during processing, making it difficult to prepare samples with identical S_a values for different loading geometries, which is essential to obtain a correct value for μ. This can be avoided by performing experiments directly under superimposed hydrostatic pressure.[40−42] Therefore, we determined μ by numerically predicting the yield data obtained from compression tests at different true strain rates and, finally, from the tensile tests under superimposed hydrostatic pressure as reported by Christiansen et al.[41] Parts a and b of Figure 6 show that an excellent description was obtained for the material parameters tabulated in Table 2 with an initial S_a value of 26.5 for the compression and 33.4 for the yield experiments, representing the difference in thermal history between the two material sets used.

To investigate whether the model is also quantitative for a different history in the postyield range, a compression sample was annealed to change its initial state. Figure 7 shows that by only slightly increasing the value of S_a from 26.5 to 29.1 it is possible to describe the intrinsic behavior of the annealed material accurately. It also should be noted that despite the difference in initial state both samples show the same rejuvenated state as was already pointed out several times before.

Until now all experimental work was based on one single polycarbonate grade, Lexan 121R. To verify whether the approach is applicable to other grades with

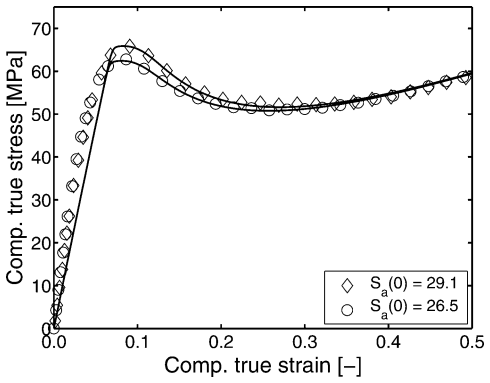

Figure 7. True stress vs true strain in uniaxial compression. Model prediction (solid lines) compared to experimental results (symbols), for different initial states at a strain rate of 10^{-4} s^{-1}.

Table 2. Material Parameters Obtained from Fitting Constant Strain-Rate Compression Data, Figure 6a, and Yield Data under Hydrostatic Pressure, Figure 6b, Using the Model

E [MPa]	ν	$\eta_{0,r}$ [MPa s]	τ_0 [MPa]	μ	S_a	r_0	r_1	r_2	G_r [MPa]
900	0.4	2.1×10^{11}	0.7	0.08	−	0.965	50	−5	26

different molecular weights and molecular weight distributions, the influence thereof on the deformation behavior was investigated. Compression, as well as tensile, samples of different polycarbonate grades were prepared and tested. To enable a proper comparison, special care was taken to ensure that all samples had the same thermal history.

From Figure 8a, it can be seen that molecular weight has no significant influence on the intrinsic deformation behavior as obtained from compression tests. This result is in agreement with the observations of van Melick et al.,[30] who performed similar experiments on polystyrene. Since compression tests cannot provide information regarding the influence of molecular weight on the strength of a material, this property was verified using tensile tests. The results of these tests, Figure 8b, show that the tensile strength increases considerably with increasing molecular weight.

4.2. Validation of Intrinsic Behavior. To validate the model, it is applied to predict the tensile behavior of samples with an arbitrary thermal history at different strain rates. Variables that depend on the postyield behavior include the draw stress after neck formation, i.e., the constant stress at which the neck propagates, and the draw ratio in the neck. Together with the yield stress, these quantities should therefore be predicted sufficiently accurately by the model. For the finite element simulations an axisymmetric model of a tensile bar with a small imperfection in the middle was used. This cylindrical tensile bar has a parallel length of 1 and a radius of 0.2. The circular imperfection has a radius of 0.02 and a maximum depth of 0.003, which is 1.5% of the bar's radius.[20] Govaert et al.[5] showed that size and shape of the imperfection have a minor influence on the deformation of the tensile bar. Only the draw ratio during stable neck growth is slightly affected. The finite element mesh consisted of 537 8-node second-order elements.[20] During the tensile test the bar is deformed at constant linear strain rates from 10^{-4} to 10^{-2} s^{-1}, similar to the actual tensile experiments.

From all the parameters in Table 2 only S_a needs to be evaluated, since it depends on the history of the

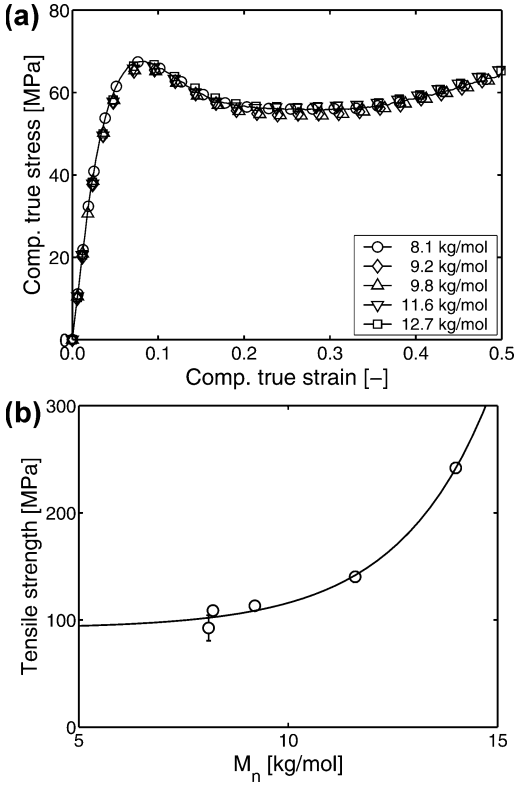

Figure 8. Influence of molecular weight M_n on the intrinsic deformation behavior (a) and tensile strength (b) of polycarbonate. Symbols indicate experimental data; solid lines are guides to the eye.

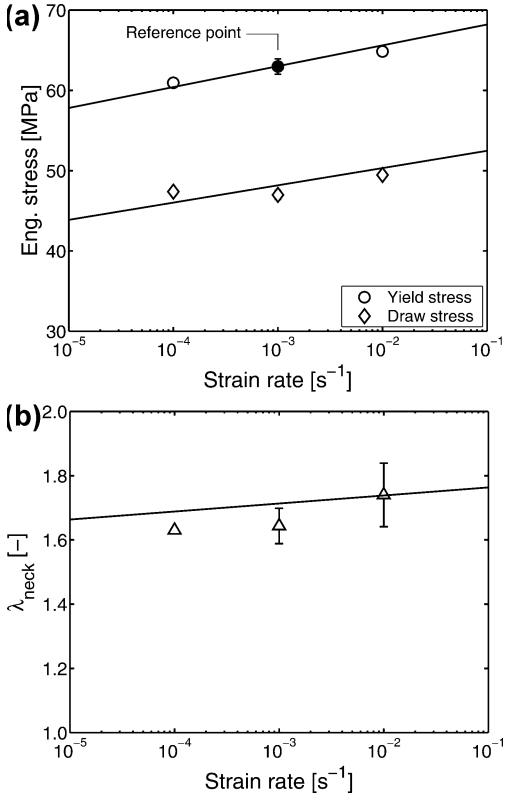

Figure 9. Validation of constitutive model, and parameter set. (a) Engineering yield and drawing stress vs strain rate, model prediction (solid lines) compared to experimental results (○, ◇). (b) Draw ratio in the neck vs strain rate, model prediction (solid line) compared to experimental data (△).

material. Fitting the model prediction to the experimentally obtained yield stress at a reference strain rate of 10^{-3} s^{-1}, an initial S_a value of 32.4 is found.

Figure 9a shows that the predicted values of both yield stresses and draw stresses, as a function of applied strain rate, compare well to the experimentally determined values. The strain rate dependence of the draw ratio in the neck is also predicted well, although the absolute value is slightly too high; see Figure 9b.

4.3. Characterization of Aging Kinetics. It was shown that the initial state of the material, S_a, can be obtained from a point-fit on the yield stress obtained from a single tensile test. Similarly the aging kinetics can be determined by monitoring the evolution of yield stress σ_y for a single strain rate, $\dot{\epsilon}_0$, with time. Since the model uses the rejuvenated state as a reference level, it seems straightforward to study the evolution of the yield stress for a rejuvenated material as a function of time. For this purpose, cylindrical samples were rejuvenated in torsion and allowed to age at room temperature for different periods of time. Subsequently, the yield stress is determined in tensile at a strain rate $\dot{\epsilon}_0$ of 10^{-2} s^{-1}. In Figure 10, the resulting yield stress can be seen to increase linearly with the logarithm of time after an initial plateau.

To describe the kinetics experimentally obtained at 23 °C, we use the following simple expression:

$$\sigma_y(t) = \sigma_{y,0} + c \log\left(\frac{t + t_a}{t_0}\right) \tag{22}$$

where $\sigma_{y,0}$, c, and t_a are fit parameters, and $t_0 = 1$ s. For the fit shown in Figure 10, $\sigma_{y,0} = 26.1$ MPa, the slope $c = 3.82$ MPa, and the initial age $t_a = 10\,715$ s.

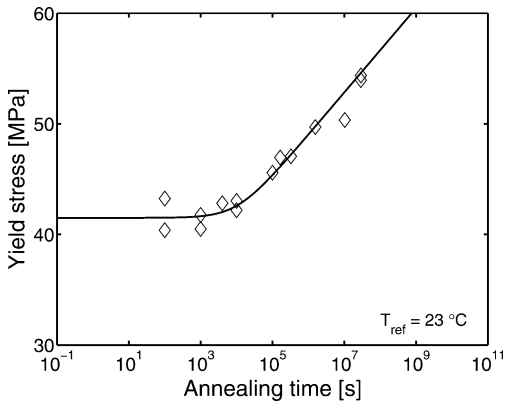

Figure 10. Evolution of yield stress at 10^{-2} s^{-1} as a function of time for mechanically rejuvenated samples at 23 °C, experimental results (◇), and fit using eq 22 (solid line).

Although the yield stress of a rejuvenated material is expected to increase from the start of aging, no change is observed during a certain (in this case relatively short) time period. This is due to the fact that the core of the cylindrical sample is not completely rejuvenated.[5] Furthermore, some heat is generated during the rejuvenation procedure, which has an accelerating effect on aging. As a result, the material already has a small initial age, t_a, and as long as the experimental time is smaller than this initial age, no aging effects are observed. This phenomenon is referred to as *progressive aging*. Something comparable was also observed by Struik[29] in the long-term creep behavior of polymers. Only for creep times longer than the age of the samples is the mechanical behavior influenced during the test.

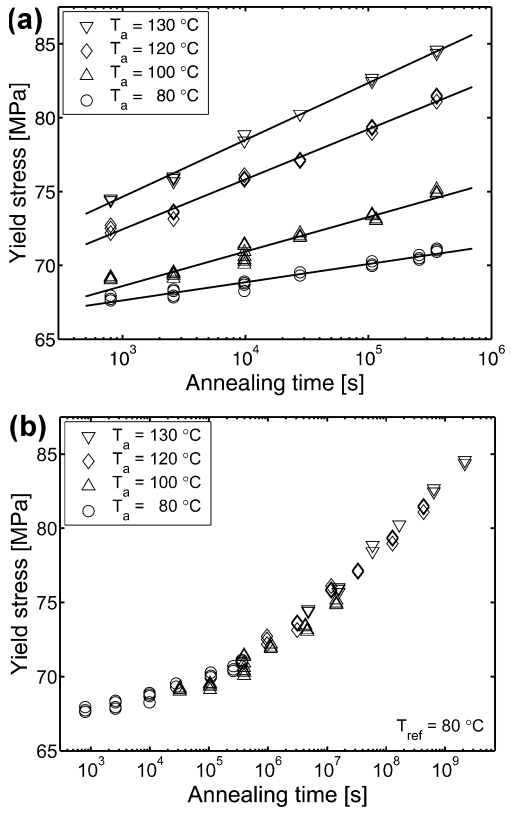

Figure 11. (a) Evolution of yield stress as a function of annealing time for different annealing temperatures. Solid lines are to guide the eye; symbols indicate experimental data. (b) Master curve for a reference temperature of 80 °C, constructed from the data in Figure 11a.

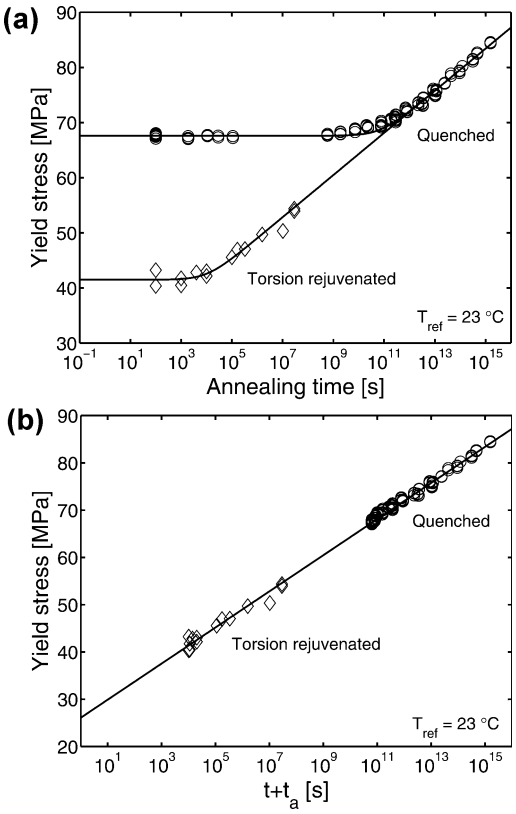

Figure 12. Evolution of yield stress of a mechanically rejuvenated material (◇), and quenched material (○) for a reference temperature of 23 °C. Solid lines are fits using eq 22.

Compared to mechanically rejuvenated samples, in practice the thermomechanical history is either less well-defined or even completely unknown, and therefore most polymers will have a more or less arbitrary initial state, e.g., after injection molding. Bauwens already showed that for an as-received polycarbonate at room temperature the yield stress did not change during a period of at least 3 years.[43] At elevated temperatures this, however, changes, and in particular for the range near the glass transition temperature, the yield stress again increases with time.[31,32] Therefore, annealing experiments on injection molded tensile bars of polycarbonate Lexan 161R were performed at different temperatures from 80 to 130 °C. Figure 11a shows the increase in yield stress with annealing time for four annealing temperatures. The increase becomes more pronounced for the higher temperatures, as was also observed by Golden et al.,[31] and Bauwens-Crowet and Bauwens.[32]

The results obtained at various temperatures can be combined into a single master curve using annealing time−temperature superposition. In Figure 11b, the resulting master curve is shown with respect to a reference temperature of 80 °C. The shift factors used to construct the master curve are accurately described by an Arrhenius relation:

$$a_T(T) = \exp\left(\frac{\Delta U_a}{R}\left(\frac{1}{T} - \frac{1}{T_{ref}}\right)\right) \qquad (23)$$

where ΔU_a denotes the activation energy, R the universal gas constant, T the annealing temperature, and T_{ref} the reference temperature (80 °C). A good description of the shift data was obtained for an activation energy ΔU_a of 205 kJ/mol. This value is only slightly smaller than the 220 kJ/mol that can be derived from the data obtained by Bauwens-Crowet and Bauwens.[32]

Special caution has to be taken when extrapolating these results to temperatures above 130 °C, since in the temperature range from 130 °C up to T_g several authors observed that an equilibrium value for the yield stress is reached.[31,32] Similar observations are reported for a DGEBA−epoxy in the range of $T_g - 10$ to T_g by Lee.[44] The equilibrium values are reported to decrease with increasing annealing temperature, as this reduces the time required to attain equilibrium. For decreasing temperatures such a plateau value may also be expected for increasing times. An onset to such a plateau value was, however, not observed in our experiments.

To enable a comparison of the master curve shown in Figure 11b with the data on the yield stress evolution of the rejuvenated samples, the master curve is shifted to a temperature of 23 °C. This comparison is shown in Figure 12a. In this figure, additional data of the same injection molded samples aged at room temperature for different times are included.

Figure 12a also shows that the data for the quenched material are described well using eq 22 with the same values for $\sigma_{y,0}$, and slope c, but with a higher initial age, t_a, of 7.3×10^{10} seconds. The value 3.82 MPa of the slope is close to that found by Hutchinson et al.[33] and LeGrand,[26] respectively 4.07, and 3.87 MPa. Furthermore, it also describes the annealing data obtained by Bauwens-Crowet and Bauwens[32] to a good approximation.

The large value for the initial age suggests that a change in yield stress can only be expected after several

centuries. This agrees well with the observations by Bauwens,[43] who saw no change in the yield stress of quenched polycarbonate that had aged for 3 years at room temperature. Furthermore, LeGrand et al.[45] did not observe a change in the impact behavior of polycarbonate that was stored for 35 years, tough still being tough.

In Figure 12b, the time scale of the experiments is compensated for the initial age t_a of the different samples. It shows that both the rejuvenated and as-received samples age at the same rate and can be described by the same kinetics. Furthermore, the figure suggests that the rejuvenated material eventually will have the same yield stress as the as-received material. This, however, seems to contradict observations by Aboulfaraj et al.,[35] on annealing a mechanically rejuvenated and as-received DGEBA diepoxy. Both types of samples showed the same aging kinetics, but differed approximately 5 MPa over the entire range of annealing times, including the equilibration plateau. No clear explanation for this difference seems at hand, except that Aboulfaraj et al. performed their experiments at the annealing temperature rather than cooling them to room temperature.

Considering the time scale of approximately 10^{11} seconds for the injection molded samples one could argue that in such case neglecting aging is a fair assumption. It is, however, also clearly demonstrated that both temperature and history have a significant effect on this time scale. Besides temperature, and history, also the load applied has a profound influence on the development in time of the yield stress. The effect of stress, or deformation, is though more controversial than that of temperature, or thermal history, as it concerns the ongoing discussion on rejuvenation vs aging. Whereas some authors claim that stress, or deformation, rejuvenates,[29,46,47] there are others who claim that stress, or deformation, accelerates aging similar to temperature.[48−54] Furthermore, there is an ongoing discussion whether either effect comprises a true structural change, or is merely a nonlinear viscoelastic effect.[55]

To study the influence of stress on the evolution of the yield stress, a constant load was applied to injection molded samples of Lexan 161R for different times at 80 °C. After the designated period, the sample was unloaded and allowed to cool to room temperature after which the yield stress was determined. The results are shown in Figure 13a. From this figure it becomes evident that an applied load enhances the increase in yield stress and that this effect is stronger for higher loads. It might be argued that the increase is due to flow induced orientational effects. Although there undoubtedly will be some orientation, the observed increase in yield stress is far greater than can be estimated on the basis of the plastic strain developed during the annealing periods.

Similar to temperature, a master curve can be created using a stress activated shift of the Eyring type (annealing time−stress superposition[56]):

$$a_\sigma(\bar{\tau}) = \frac{\bar{\tau}/\tau_a}{\sinh(\bar{\tau}/\tau_a)} \quad \text{with} \quad \tau_a = \frac{RT}{\bar{\nu}_a} \tag{24}$$

where an (aging) activation volume $\bar{\nu}_a = 1.33 \times 10^{-3}$ m^3/mol follows from fitting the shift data, and $\bar{\tau}$ is the equivalent stress applied. Figure 13b shows that these

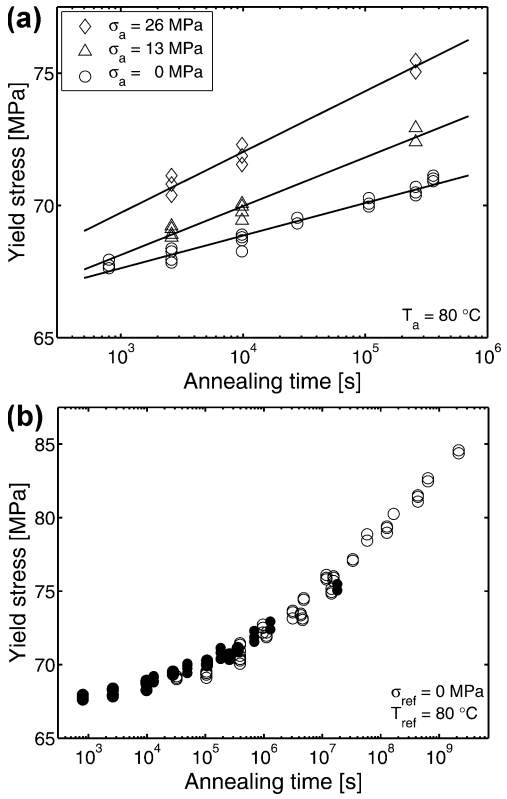

Figure 13. (a) Evolution of yield stress as a function of annealing time for different stresses at 80 °C. Solid lines are to guide the eye, symbols indicate experimental data. (b) Master curve constructed from the data in part a for a reference stress of 0 MPa and 80 °C (●), compared to the master curve obtained from temperature data only (○).

curves can indeed be superimposed to form a master curve. Moreover, this master curve coincides with that previously obtained for temperature annealing.

This result allows the description of a thermomechanical history using a single master curve, combined with a temperature and stress dependent shift function, which, for a constant strain rate $\dot{\epsilon}_0$, leads to the following equation for S_a (see Appendix):

$$S_a(t_{eff}) = c_0 + c_1 \log\left(\frac{t_{eff}(t, T, \bar{\tau}) + t_a}{t_0}\right) \tag{25}$$

where

$$c_0 = \frac{\sqrt{3}+\mu}{3\tau_0}\left(\sigma_{y,0}(\dot{\epsilon}_0) - \sigma_{rej}(\dot{\epsilon}_0) - \frac{\sqrt{3}}{\sqrt{3}+\mu}\sigma_r(\lambda_y)\right) \tag{26}$$

$$c_1 = \frac{\sqrt{3}+\mu}{3\tau_0}\, c \tag{27}$$

and the effective time, t_{eff}, is defined as

$$t_{eff}(t, T, \bar{\tau}) = \int_0^t \frac{d\xi}{a_T(T(\xi))\, a_\sigma(\bar{\tau}(\xi))} \tag{28}$$

where a_T and a_σ are given by eqs 23 and 24, respectively. For a reference temperature of 23 °C and strain rate $\dot{\epsilon}_0$ of 10^{-2} s^{-1} the values for c_0 and c_1 equal −4.41 and 3.3, respectively.

To verify the applicability of these results to other grades, more specifically other molecular weights, the

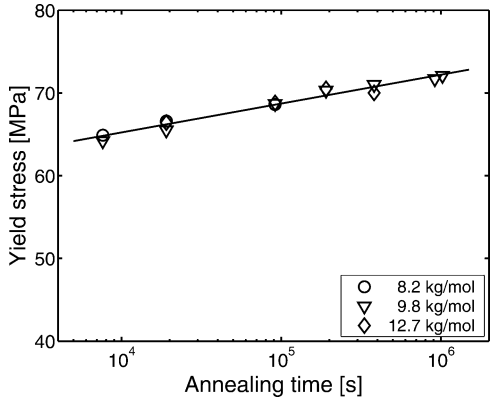

Figure 14. Yield stress vs annealing time for different grades of polycarbonate annealed at 120 °C. Symbols indicate experimental data; the solid line is a guide to the eye.

Table 3. Material Parameters for Polycarbonate at a Reference Temperature of 23 °C

E [MPa]	ν	$\eta_{0,r}$ [MPa s]	τ_0 [MPa]	μ	S_a	r_0	r_1	r_2	G_r [MPa]
900	0.4	2.1×10^{11}	0.7	0.08	−	0.965	50	−5	26

c_0	c_1	t_a [s]	ΔU_a [kJ/mol/K]	$\bar{v}_a$ [m^3/mol]
−4.41	3.3	−	205	1.33×10^{-3}

aging kinetics of several different polycarbonate grades were studied at a temperature of 120 °C. From Figure 14, it is clear that the resulting annealing kinetics are independent of molecular weight.

This is according to expectation, since the evolution of yield stress is associated with segmental molecular motion and should, therefore, not be influenced by molecular weight. Similar results were found by Ryan[57] for annealing two polycarbonates with different molecular weights at 125 °C. Although there is a small vertical offset between the curves, which could be due to a difference in thermal history, the slope is the same.

To conclude this part we summarized all relevant parameters for polycarbonate in Table 3, with exception of values for the parameter S_a, the initial value for S, or, alternatively the initial age t_a, as these are determined for each material separately, using the yield stress at a reference strain-rate.

4.4. Validation of Aging Kinetics. To validate the expressions determined for the aging kinetics, the evolution of the yield stress of injection molded Lexan 141R was studied for two different initial states, obtained by using two different mold temperatures, 25 and 140 °C. Subsequently, samples from both initial states were annealed at temperatures from 80 to 130 °C for increasing annealing times. Using the previously obtained temperature shift expression (eq 23) and activation energy, two master curves were constructed which are shown in Figure 15a. Finally, for both types, the initial age t_a (rather than S_a, since we used eq 22) was determined from a single tensile test at a strain rate of 10^{-2} s^{-1}, and substituted in eq 22.

Figure 15a clearly shows that the difference in mold temperature has led to a significant difference in the initial age and thus initial yield stress of the samples. The initial age (at 80 °C) of the samples from the hot mold (140 °C) is about 15 times higher than that of the samples from the cold mold (25 °C). Therefore, the yield stress of the latter samples starts to increase first, and finally coincides with the increasing yield stresses of the other samples. From the figure, it is also clear that this behavior is captured well by the model.

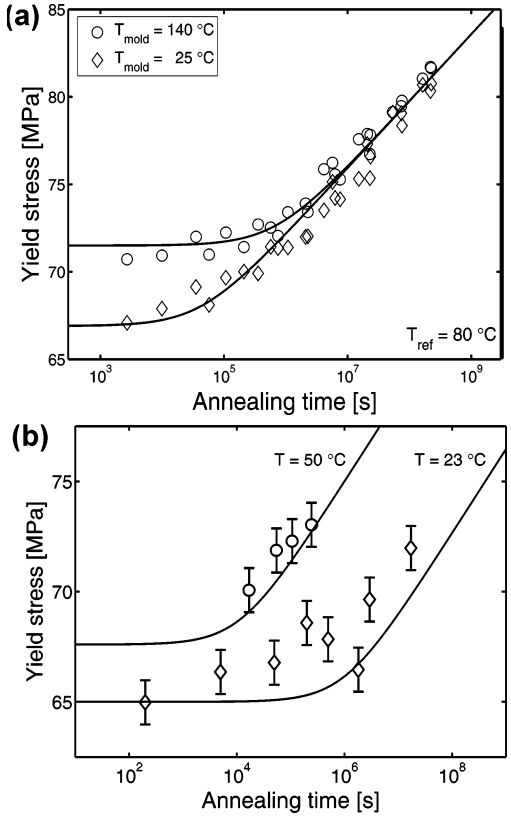

Figure 15. Evolution of yield stress as a function of time: (a) PC Lexan 141R having two different initial ages; (b) polycarbonate under the influence of combined temperature and stress (40 MPa). Symbols indicate experimental data and solid lines are model predictions.

In a second type of validation experiment, injection molded samples were subjected to a constant load of 40 MPa at two different temperatures (23 and 50 °C) for different annealing times. For both combinations the evolution of the yield stress is shown in Figure 15b, together with the prediction by the model. For both cases, the yield stress is constant at first and then evolves with time, the evolution starting at shorter times for the higher temperature. The model appears to capture the trend in the evolution fairly well, although for room temperature the time scale is slightly overpredicted. It should, however, be noted that the selected test conditions are far outside the experimental window used to determine the material parameters used for this prediction.

5. Conclusions

In this investigation a first attempt is made to introduce aging kinetics in the existing 3D elastoviscoplastic constitutive models. To achieve this, the driving stress was assumed to consist of a history independent rejuvenated stress, which acts as a reference level for the history dependent yield drop. The evolution of the yield drop, which is the increase in yield stress with time due to aging, is determined by a single state parameter S that depends on time, temperature, stress, and plastic strain. To a first approximation the aging and rejuvenation kinetics are represented by two decoupled expressions. Although this limits the applicability, it greatly facilitates the determination of the relevant kinetics.

The relevant softening kinetics could be extracted from the intrinsic deformation behavior determined in uniaxial compression, and a suitable expression to describe the kinetics was selected. Some material parameters were obtained from the literature (like the strain hardening modulus and Poisson's ratio), the remainder was determined experimentally from compression tests at different strain rates. The resulting parameter set was shown to be able to correctly predict the strain rate dependence of yield stress, draw stress, and the draw ratio in the neck for a material with an arbitrary initial state, which was obtained from a single tensile test.

Aging kinetics were determined by monitoring the evolution of the yield stress for mechanically rejuvenated, and quenched, polycarbonate samples. It was shown that, except for a pronounced difference in initial age, both types of samples had the same aging kinetics. Moreover, the evolution of the yield stress of the rejuvenated samples appeared to coincide with that of the quenched samples for very long times. The resulting kinetics are described with a single expression with different initial ages. Furthermore, it was shown that aging kinetics are accelerated both by temperature, and stress. For each, appropriate shift functions were derived including the material parameters. In combination with the expression for the aging kinetics it proved possible to describe the evolution of the yield stress of polycarbonate samples subjected to very different thermomechanical histories.

The influence of the molecular weight on the intrinsic deformation behavior, aging kinetics, and strength was shown. As expected, both the intrinsic deformation behavior, and aging kinetics were independent of molecular weight. This simplifies the characterization of different polymers tremendously, since almost all parameters in the constitutive model need to be determined once only, for every polymer. Only the tensile strength showed a clear dependence on molecular weight, which is important for the development of a final failure criterion.

As a last remark, it should be noted that changes in the structural state also lead to changes in properties other than the yield stress, for example enthalpy overshoot and specific volume. In literature, a qualitative relation has been reported between the change in yield stress and the change in enthalpy,[58] which suggests a possible relation between our empirical state parameter S and the level of enthalpy overshoot. Unfortunately, however, the empirical nature of our constitutive approach does not supply us a physical basis to directly relate these quantities. With respect to specific volume, the observed increase in density during mechanical rejuvenation[30] clearly implies that there is no direct relation to yield stress or to the state parameter S.

Acknowledgment. The authors wish to acknowledge Bas Raas and Chris van Haag for their important contributions to the experimental work.

Appendix: Aging Kinetics

Under the assumption that at the yield point the material behaves incompressible, it is possible to derive a simple linear relationship between the tensile yield stress $\sigma_y(t)$ at a constant rate of deformation $\dot{\epsilon}_0$ and $S_a(t)$.

For incompressible behavior the total stress $\boldsymbol{\sigma}$ can be described by

$$\boldsymbol{\sigma} = -p\boldsymbol{I} + 2\eta\boldsymbol{D}_p + G_r\boldsymbol{B}^d \tag{29}$$

where the unknown hydrostatic pressure p follows from the boundary conditions, the second term represents the flow contribution with viscosity η, defined by eq 16, and the last term representing the strain hardening contribution with modulus G_r.

For uniaxial deformation under a constant strain rate, we find for the resulting stress σ and hydrostatic pressure p:

$$\sigma = 3\eta\dot{\epsilon}_p + G_r(\lambda^2 - \lambda^{-1}) \tag{30}$$

$$p = -\eta\dot{\epsilon}_p - \frac{1}{3}G_r(\lambda^2 - \lambda^{-1}) = -\frac{1}{3}\sigma \tag{31}$$

where $\dot{\epsilon}_p$ is the plastic strain rate, and λ is the draw ratio.

It is assumed that at the yield point (λ_y, σ_y) (i) the plastic strain rate equals the applied strain rate $\dot{\epsilon}_0$, (ii) the softening expression $R_\gamma = 1$ and, therefore, $S = S_a(t)$, and (iii) the argument of the hyperbolic sine in the viscosity function is large and therefore may be approximated by an exponential function.

Incorporation of these considerations and rewriting yield for the viscosity

$$\eta = \frac{\tau_0}{\sqrt{3}\dot{\epsilon}_0}\left[\ln\left(2\sqrt{3}\frac{\eta_{0,r}}{\tau_0}\dot{\epsilon}_0\right) + S_a(t) + \frac{\mu p}{\tau_0}\right] \tag{32}$$

and combined with eqs 30 and 31, this results in

$$\sigma_y(t) = \sigma_{rej}(\dot{\epsilon}_0) + \frac{3\tau_0}{\sqrt{3}+\mu}S_a(t) + \frac{\sqrt{3}}{\sqrt{3}+\mu}\sigma_r(\lambda_y) \tag{33}$$

where

$$\sigma_{rej}(\dot{\epsilon}_0) = \frac{3\tau_0}{\sqrt{3}+\mu}\ln\left(2\sqrt{3}\frac{\eta_{0,r}}{\tau_0}\dot{\epsilon}_0\right) \tag{34}$$

$$\sigma_r(\lambda_y) = G_r({\lambda_y}^2 - {\lambda_y}^{-1}) \tag{35}$$

Together with the experimentally obtained evolution equation for the yield stress (eq 22), this leads to

$$S_a(t) = c_0 + c_1\log\left(\frac{t+t_a}{t_0}\right) \tag{36}$$

with

$$c_0 = \frac{\sqrt{3}+\mu}{3\tau_0}\left[\sigma_{y,0} - \sigma_{rej}(\dot{\epsilon}_0) - \frac{\sqrt{3}}{\sqrt{3}+\mu}\sigma_r(\lambda_y)\right] \tag{37}$$

$$c_1 = \frac{\sqrt{3}+\mu}{3\tau_0}c \tag{38}$$

References and Notes

(1) Haward, R.; Thackray, G. *Proc. R. Soc. London A* **1968**, *302*, 453−472.
(2) Boyce, M. C.; Parks, D. M.; Argon, A. S. *Mech. Mater.* **1988**, *7*, 15−33.
(3) Wu, P. D.; van der Giessen, E. *J. Mech. Phys. Solids* **1993**, *41*, 427−456.
(4) Buckley, C. P.; Jones, D. C. *Polymer* **1995**, *36*, 3301−3312.

(5) Govaert, L. E.; Timmermans, P. H. M.; Brekelmans, W. A. M. *J. Eng. Mater. Techn.* **2000**, *122*, 177−185.
(6) Meijer, H. E. H.; Govaert, L. E. *Macromol. Chem. Phys.* **2003**, *204*, 274−288.
(7) Eyring, H. *J. Chem. Phys.* **1963**, *4*, 283−295.
(8) Treloar, L. R. G. *The Physics of Rubber Elasticity*; Clarendon Press: Oxford, England, 1975.
(9) Argon, A. S. *Philos. Mag.* **1973**, *28*, 839−865.
(10) Wang, M. C.; Guth, E. J. *J. Chem. Phys.* **1952**, *20*, 1144−1157.
(11) Arruda, E. M.; Boyce, M. C. *Int. J. Plast.* **1993**, *9*, 783−811.
(12) Tervoort, T. A.; Smit, R. J. M.; Brekelmans, W. A. M.; Govaert, L. E. *Mech. Time-Dep. Mater.* **1998**, *1*, 269−291.
(13) Leonov, A. I. *Rheol. Acta* **1976**, *15*, 85−98.
(14) Baaijens, F. P. T. *Rheol. Acta* **1991**, *30*, 284−299.
(15) Hasan, O. A.; Boyce, M. C.; Li, X. S.; Berko, S. *J. Polym. Sci., Part B: Polym. Phys.* **1993**, *31*, 185−197.
(16) Tervoort, T. A.; Govaert, L. E. *J. Rheol.* **2000**, *44*, 1263−1277.
(17) Wu, P. D.; van der Giessen, E. *Int. J. Sol. Struct.* **1993**, *31*, 1493−1517.
(18) Wu, P. D.; van der Giessen, E. *Int. J. Plast.* **1993**, *11*, 211−235.
(19) Meijer, H. E. H.; Govaert, L. E.; Smit, R. J. M. Multi-Level Finite Element Method for Modelling Rubber-Toughened Amorphous Polymers. In *Toughening of Plastics*; Pearson, R. A., Ed.; American Chemical Society: Washington, DC, 1999.
(20) Van Melick, H. G. H.; Govaert, L. E.; Meijer, H. E. H. *Polymer* **2003**, *44*, 3579−3591.
(21) Adam, G. A.; Cross, A.; Haward, R. N. *J. Mater. Sci.* **1975**, *10*, 1582−1590.
(22) Cross, A.; Haward, R. N. *Polymer* **1978**, *19*, 677−682.
(23) G'Sell, C. Plastic deformation of glassy polymers: constitutive equations and macromolecular mechanisms. In *Strength of Metals and Alloys*; McQueen, H. J., et al., Eds.; Pergamon Press: Oxford, England, 1986.
(24) Bauwens, J.-C. *J. Mater. Sci.* **1978**, *13*, 1443−1448.
(25) Govaert, L. E.; van Melick, H. G. H.; Meijer, H. E. H. *Polymer* **2001**, *42*, 1271−1274.
(26) LeGrand, D. G. *J. Appl. Polym. Sci.* **1969**, *13*, 2129−2147.
(27) Hill, A. J.; Heater, K. J.; Agrawal, C. M. *J. Polym. Sci., Part B: Polym. Phys.* **1990**, *28*, 387−405.
(28) Bubeck, R. A.; Bales, S. E.; Lee, H.-D. *Polym. Eng. Sci.* **1984**, *24*, 1142−1148.
(29) Struik, L. C. E. *Physical Aging in Amorphous Polymers and other Materials*; Elsevier: Amsterdam, 1978.
(30) Van Melick, H. G. H.; Govaert, L. E.; Raas, B.; Nauta, W. J.; Meijer, H. E. H. *Polymer* **2003**, *44*, 1171−1179.
(31) Golden, J. H.; Hammant, B. L.; Hazell, E. A. *J. Appl. Polym. Sci.* **1967**, *11*, 1571−1579.
(32) Bauwens-Crowet, C.; Bauwens, J.-C. *Polymer* **1982**, *23*, 1599−1604.
(33) Hutchinson, J. M.; Smith, S.; Horne, B.; Gourlay, G. M. *Macromolecules* **1999**, *32*, 5046−5061.
(34) Bauwens-Crowet, C.; Bauwens, J.-C. *Polymer* **1988**, *29*, 1985−1989.
(35) Aboulfaraj, M.; G'Sell, C.; Mangelinck, D.; McKenna, G. B. *J. Non-Cryst. Solids* **1994**, *172−174*, 615−621.
(36) G'Sell, C.; Hiver, J. M.; Dahoun, A.; Souahi, A. *J. Mater. Sci.* **1992**, *27*, 5031−5039.
(37) Macosko, C. W. *Rheology; Principles, Measurements, and Applications*; VCH Publishers: New York, 1994.
(38) Bauwens-Crowet, C.; Bauwens, J.-C.; Homès, G. *J. Mater. Sci.* **1972**, *7*, 176−183.
(39) Govaert, L. E.; Schellens, H. J.; Thomassen, H. J. M.; Smit, R. J. M.; Terzoli, L.; Peijs, T. *Composites: Part A* **2001**, *32*, 1697−1711.
(40) Sauer, J. A.; Mears, D. R.; Pae, K. D. *Eur. Polym. J.* **1970**, *6*, 1015−1032.
(41) Christiansen, A. W.; Baer, E.; Radcliffe, S. V. *Philos. Mag.* **1971**, *24*, 451−467.
(42) Spitzig, W. A.; Richmond, O. *Polym. Eng. Sci.* **1979**, *19*, 1129−1139.
(43) Bauwens, J.-C. *Plast. Rubber Proc. Appl.* **1987**, *7*, 143−147.
(44) Lee, A.; McKenna, G. B. *Polymer* **1988**, *29*, 1812−1817.
(45) LeGrand, D. G.; Miller, S.; McCloskey, P. Long-term room-temperature aging of polycarbonate resins. In *Abstract book 74th Annual Meeting Society of Rheology*; Co, A., Ed.; Society of Rheology: Minneapolis, MN, 2002.
(46) Ricco, T.; Smith, T. L. *Polymer* **1985**, *26*, 1979−1984.
(47) Pixa, R.; Le Dû, V.; Wippler, C. *Colloid Polym. Sci.* **1988**, *266*, 913−920.
(48) Vincent, P. I. *Polymer* **1960**, *1*, 7−19.
(49) Kramer, E. J. *J. Appl. Phys.* **1970**, *41*, 4327−4341.
(50) Struik, L. C. E. *Polymer* **1980**, *21*, 962−967.
(51) Nanzai, Y.; Miwa, A.; Cui, S. Z. *Polym. J.* **2000**, *32*, 51−56.
(52) Nanzai, Y.; Cui, S. Z. *J. Polym. Sci.: Part B: Polym. Phys.* **2001**, *33*, 444−449.
(53) Cui, S. Z.; Nanzai, Y.; Yoshioka, S. *Kobunshi Ronbunshu* **2000**, *57*, 37−44.
(54) Sternstein, S. S. *Polym. Prepr.* **1976**, *17*, 136−141.
(55) McKenna, G. B. *J. Phys.: Condens. Matter* **2003**, *15*, 737−763.
(56) Tervoort, T. A.; Klompen, E. T. J.; Govaert, L. E. *J. Rheol.* **1996**, *40*, 779−797.
(57) Ryan, J. T. *Polym. Eng. Sci.* **1978**, *18*, 264−267.
(58) Aref-Azar, A.; Biddlestone, F.; Hay, J. N.; Haward, R. N. *Polymer* **1983**, *24*, 1245−1251.

MA050498V